www.czasopisma.pan.pl PAN POLSKA AKADEMIA NAUK www.journals.pan.pl

Arch. Metall. Mater. **63** (2018), 3, 1467-1471

DOI: 10.24425/123831

A. ZAKIYUDDIN*, K. LEE*#

MICROSTRUCTURE AND CORROSION BEHAVIORS OF BIODEGRADABLE Mg-1Zn-1Zr-xSn ALLOYS PREPARED BY POWDER-IN-TUBE ROLLING

The objective of the present study was to investigate the effects of Sn addition on the mechanical and corrosion properties of Mg-1Zn-1Zr-xSn (x = 1, 2, 3, 4, 5 wt.%) alloys prepared by powder-in-tube rolling (PTR) method. The PTR-treated Mg alloys reached 98.3% of theoretical density. The hardness of the alloy increased with Sn addition. Two main intermetallic phases, Mg_2Sn and Zn_2Zr_3, were formed in the alloys. The Mg_2Sn intermetallic particles were observed along the grain boundaries, while the Zn_2Zr_3 particles were distributed in the Mg matrix. The addition of 1 wt. % Sn caused the corrosion potential to shift toward a more positive value, and the resulting alloy exhibited low corrosion current density.

Keywords: Biodegradable Mg alloy, Powder-in-tube rolling, Corrosion behavior

1. Introduction

The excellent biocompatibility and biodegradability of Mg alloys make them promising candidates for metallic biodegradable materials [1,2]. Unfortunately, Mg-based implants degrade rapidly in a physiological environment, which leads to failure of the implants before the tissues are completely healed [3-5]. In addition, the relatively low mechanical strength of magnesium limits its load bearing applications. Therefore, to use Mg for biodegradable implants, its strength, elongation, and corrosion resistance must be improved [6-8]. Sn has been proven to improve localized-corrosion resistance and inhibit cathodic H_2 evolution in Mg-based alloys [9,10]. When mechanical integrity is the most consideration, a reduction in corrosion of the Sn-containing Mg alloy can also help maintain the mechanical properties of the material, Sn and Zn can also increase the strength of Mg alloys via solid solution strengthening [11].

Common fabrication methods for Mg-based alloys include various type of casting methods, which require an inert environment due to the self-ignition of Mg at 473°C in oxygen-rich environments. This makes it difficult and expensive to fabricate Mg-based alloys by conventional methods. Conventional powder metallurgy (PM) processes result in the instantaneous formation of an oxide layer (3-5nm) upon exposure to air [12]. In addition, uniaxial compaction is not effective in breaking the oxide layer.

Compared to the casting methods and the conventional PM process, the powder-in-tube rolling (PTR) process [13,14] requires a strictly controlled environment that makes it suitable for fabricating Mg-based alloys. To date, there have been no reports regarding the fabrication of Mg-based alloys via PTR. Therefore, in the present study, the microstructure and corrosion properties of Mg-1Zn-1Zr-xSn (x = 1, 2, 3, 4, 5 wt.%) alloy prepared using PTR were investigated. In addition, the effects of Sn addition on the mechanical and corrosion properties of the resulting alloy are discussed.

2. Experimental

Magnesium powder (99.6%, –100+200 mesh, Alfa Aesar), zinc powder (99.9%, –200 mesh, Alfa Aesar), zirconium powder (99.98%, –200 mesh, Alfa Aesar), and tin powder (99.8%, –200 mesh, Alfa Aesar) were used for preparation of the alloys. Mg-1wt. %Zn-1wt. %Zr-xSn (x = 1, 2, 3, 4, 5 wt. %) quaternary alloys were prepared using the PTR method. Fig. 1 shows a schematic diagram of the PTR method. The powder mixtures were first compacted and sealed inside a stainless steel tube. Hot rolling was performed at a temperature of 450°C with a reduction ratio of 82.6%. The rolled specimens were sintered at a temperature of 550°C for 6 h. The sheath was then peeled off to expose the magnesium alloys for further evaluation. The chemical compositions of the specimens are presented in Table 1.

The microstructures of the sintered specimens were observed by using an optical microscope (DM2700, Leica, Germany) and a scanning electron microscope (S-4700, HITACHI, Japan) equipped with an energy dispersive X-ray spectroscopy

* SCHOOL OF MATERIALS SCIENCE & ENGINEERING, CHONNAM NATIONAL UNIVERSITY, GWANGJU 61186, REPUBLIC OF KOREA

Corresponding author: kmlee@jnu.ac.kr

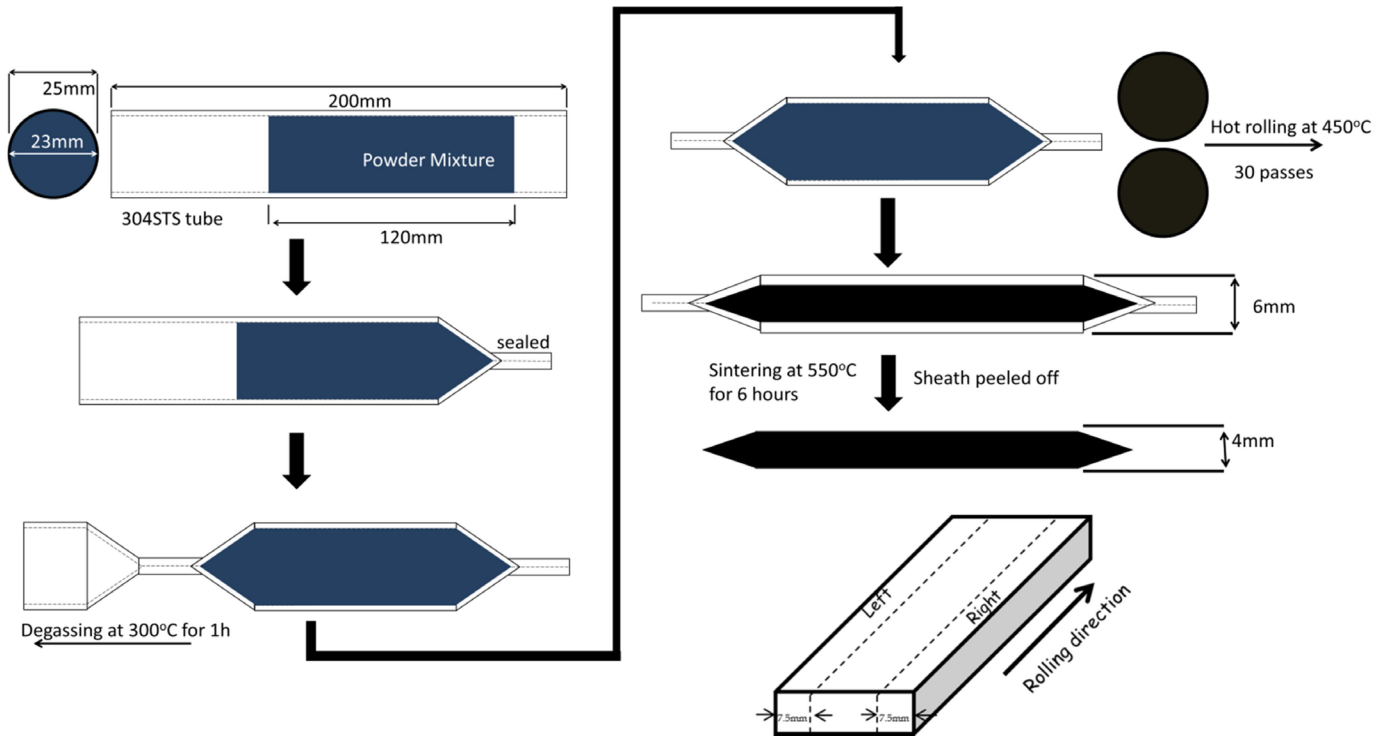

Fig. 1. Schematic diagram of the powder-in-tube rolling (PTR) method

(EDS) system. X-ray diffractometry (X-Ray Diffractometer, DMAX/1200, Rigaku, Japan) was used to determine the phases present in the specimens, using Cu Kα radiation generated at 40 kV and 35 mA.

TABLE 1

Chemical compositions of the alloys

	Mg (%)	Zn (%)	Zr (%)	Sn (%)	Theoretical density (g/cm^3)
1Sn	Bal.	1	1	1	1.778
2Sn	Bal.	1	1	2	1.792
3Sn	Bal.	1	1	3	1.806
4Sn	Bal.	1	1	4	1.82
5Sn	Bal.	1	1	5	1.835

The electrochemical tests were conducted in a flat cell containing 300 mL of a Tas simulated body fluid (Tas-SBF) solution with the chemical composition listed in Table 2 [15]. The Tas-SBF solution had a pH of 7.41 and temperature of 37±1°C, as measured by a PARSTAT 2273 potentiostat/galvanostat (Princeton Applied Research). Three-electrode cells were used for the potentiodynamic polarization tests (PDP). A silver/silver chloride electrode (SSC) in saturated KCl solution was used as a reference electrode, and the counter electrode was made of a platinum plate; the magnesium alloys were used as the working electrodes. The experiments were performed at a constant scan rate of 0.25 mV/s initiated at −250 mV below the open-circuit potential.

TABLE 2

Chemical composition of the Tas-SBF and comparison to human blood plasma

Solution	Ion concentration (mmol/L)							
	Na^+	K^+	Mg^{2+}	Ca^{2+}	Cl^-	HCO_3^-	HPO_4^{2-}	SO_4^{2-}
Blood plasma	142	5	1.5	2.5	103	27	1	0.5
Tas SBF	142	5	1.5	2.5	125	27	1	0.5

3. Results and discussion

Fig. 2 shows the optical micrographs of the PTR treated specimens. The porosities of the specimens differed according to section of the material because of the nature of the rolling process. The porosity of the edge sections was high, while that of the center section was dense. During the rolling process, the center section of the specimen was more heavily deformed as compared to the edge section. The grains of the PTR treated specimens were elongated along the rolling direction and were uniform in size. The primary fine grains were formed in the powder particles. The average size of the primary grains was 40.9 μm. The measured densities of the PTR treated specimens are listed in Table 3.

The density measurements of PTR treated specimens were divided into 3 sections: left and right edges, and center section. The density of the center section was approximately 98% of the theoretical value, which was the highest among 3 sections. Because of the lower density of both edge sections, only the center section of the specimens was used for further evaluation.

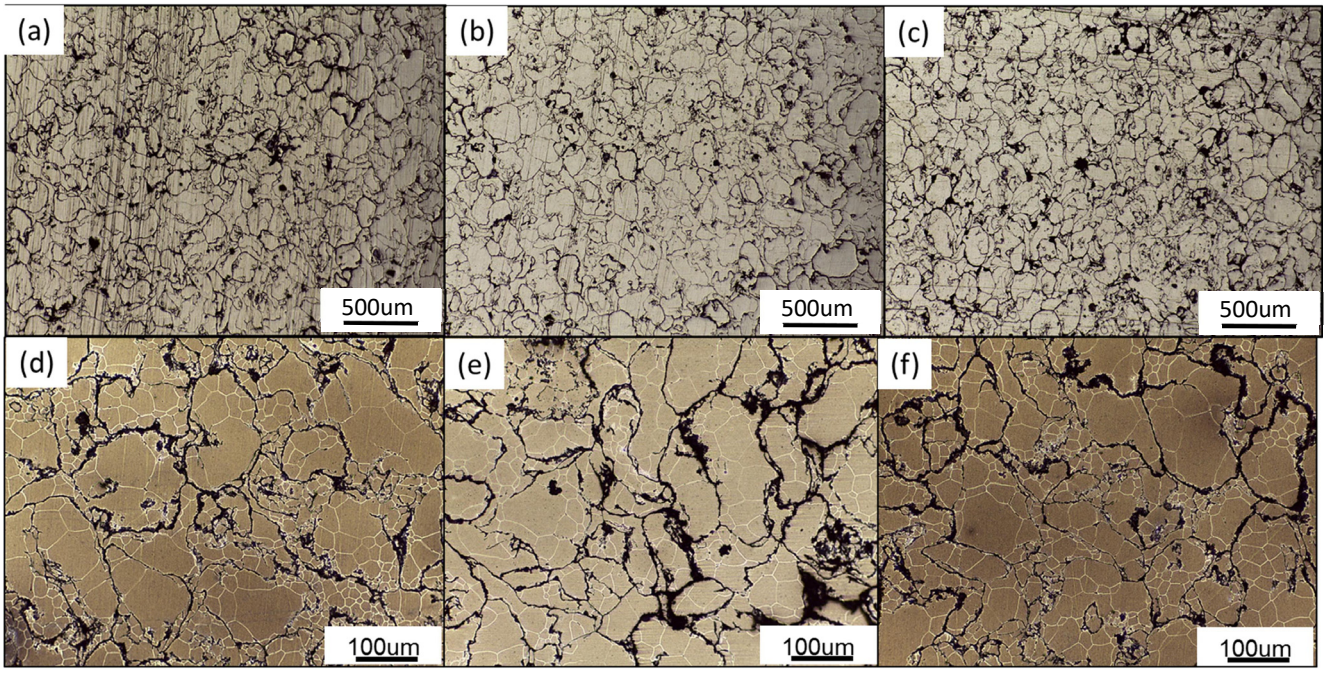

Fig. 2. Optical micrographs of the PTR treated Mg-1Zn-1Zr-5Sn alloys: (a) left section, (b) center section, (c) right section, (d) higher magnification image of a, (e) higher magnification image of b, and (f) higher magnification image of c

TABLE 3

Measured densities of the Mg-1Zn-1Zr-xSn alloys processed by powder-in-tube rolling

	1Sn	2Sn	3Sn	4Sn	5Sn
Left	93.89%	94.32%	93.26%	92.85%	95.49%
Center	98.56%	98.38%	97.21%	97.95%	98.77%
Right	92.64%	93.57%	95.64%	95.21%	94.56%
average	95.03%	95.42%	95.37%	95.34%	96.27%

SEM images of the PTR-processed Mg-1Zn-1Zr-5Sn are shown in Fig. 3. The distribution of the intermetallic phases was relatively uniform. EDX analysis revealed that a large fraction of the Sn was found in the intermetallic phases along the grain boundaries, while Zn and Zr were not found in these areas. The ratio between Mg and Sn implied a stoichiometry of Mg_2Sn. Large fractions of Zn and Zr were observed inside the Mg matrix and were identified as Zn_2Zr_3 intermetallic compounds.

Fig. 4 shows the XRD diffraction patterns of PTR treated specimens. The Mg_2Sn and Zn_2Zr_3 intermetallic particles were formed in all specimens. The addition of Zr suppressed the formation of the $MgZn_2$ intermetallic phase and promoted the formation of the Zn_2Zr_3 phase [16]. The Mg_2Sn intermetallic phase became more abundant as the amount of Sn was increased.

Fig. 5 shows Vickers hardness values of the PTR treated specimens. The Vickers indentation was obtained along the rolling direction and perpendicular to the rolling direction. Higher hardness was obtained at the center of PTR treated specimens. The hardness value of the specimens was increased with increasing Sn content in the alloys. The highest hardness of 75 HV was obtained for the Mg-1Zn-1Zr-5Sn alloy, because of the presence of the distributed intermetallic particles in the matrix and along the grain boundaries.

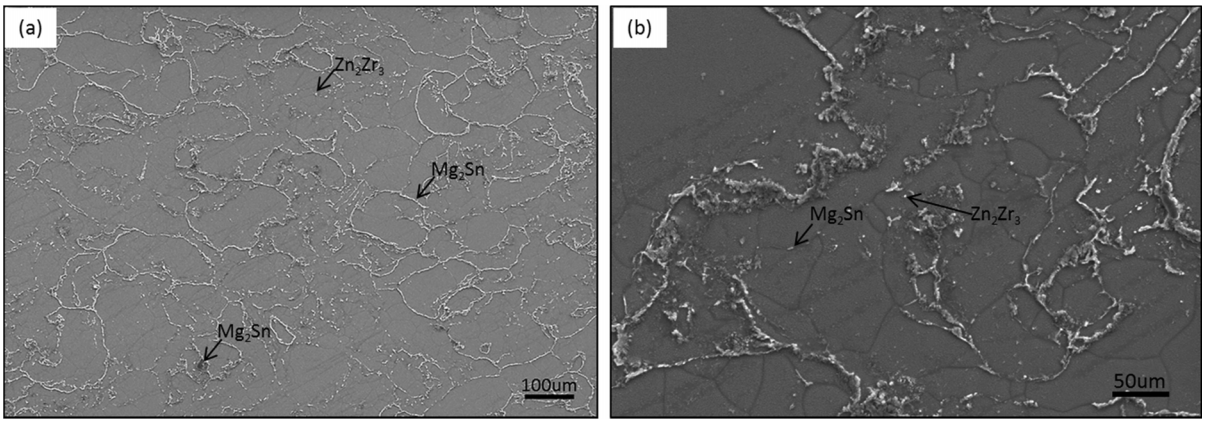

Fig. 3. SEM images of the center section of the Mg-1Zn-1Zr-5Sn alloy: (a) 500× magnification and (b) 1000× magnification

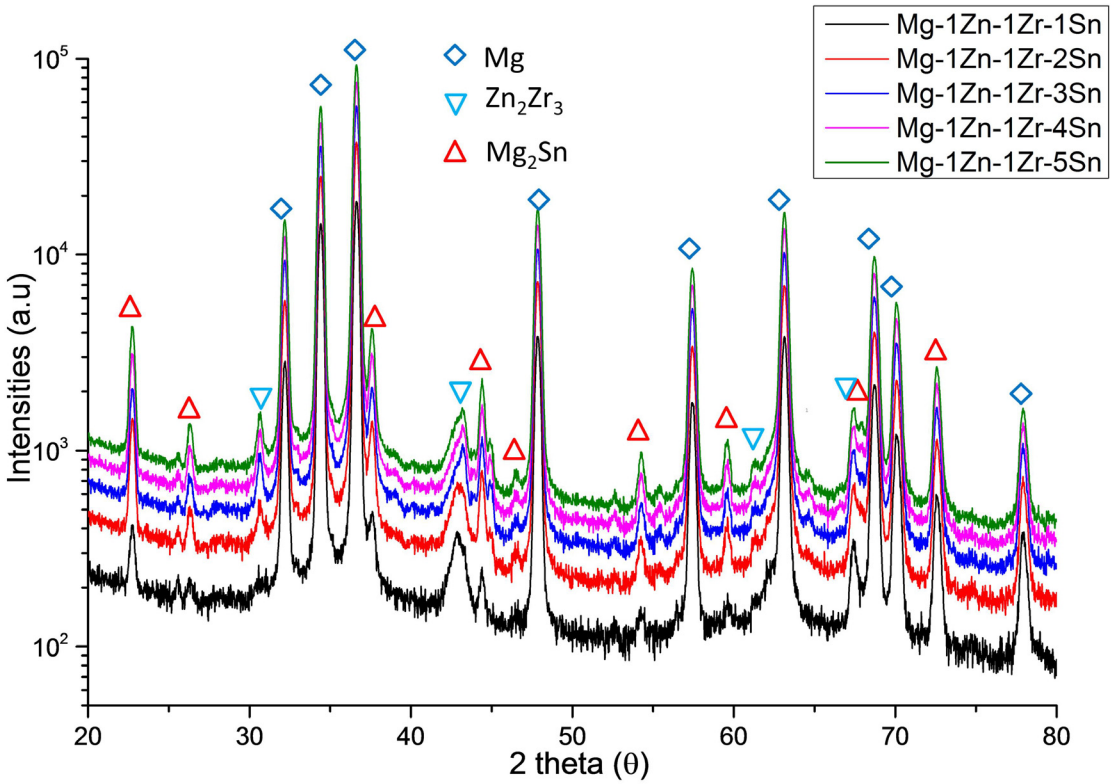

Fig. 4. X-ray diffraction pattern of the PTR treated Mg-1Zn-1Zr-xSn alloys

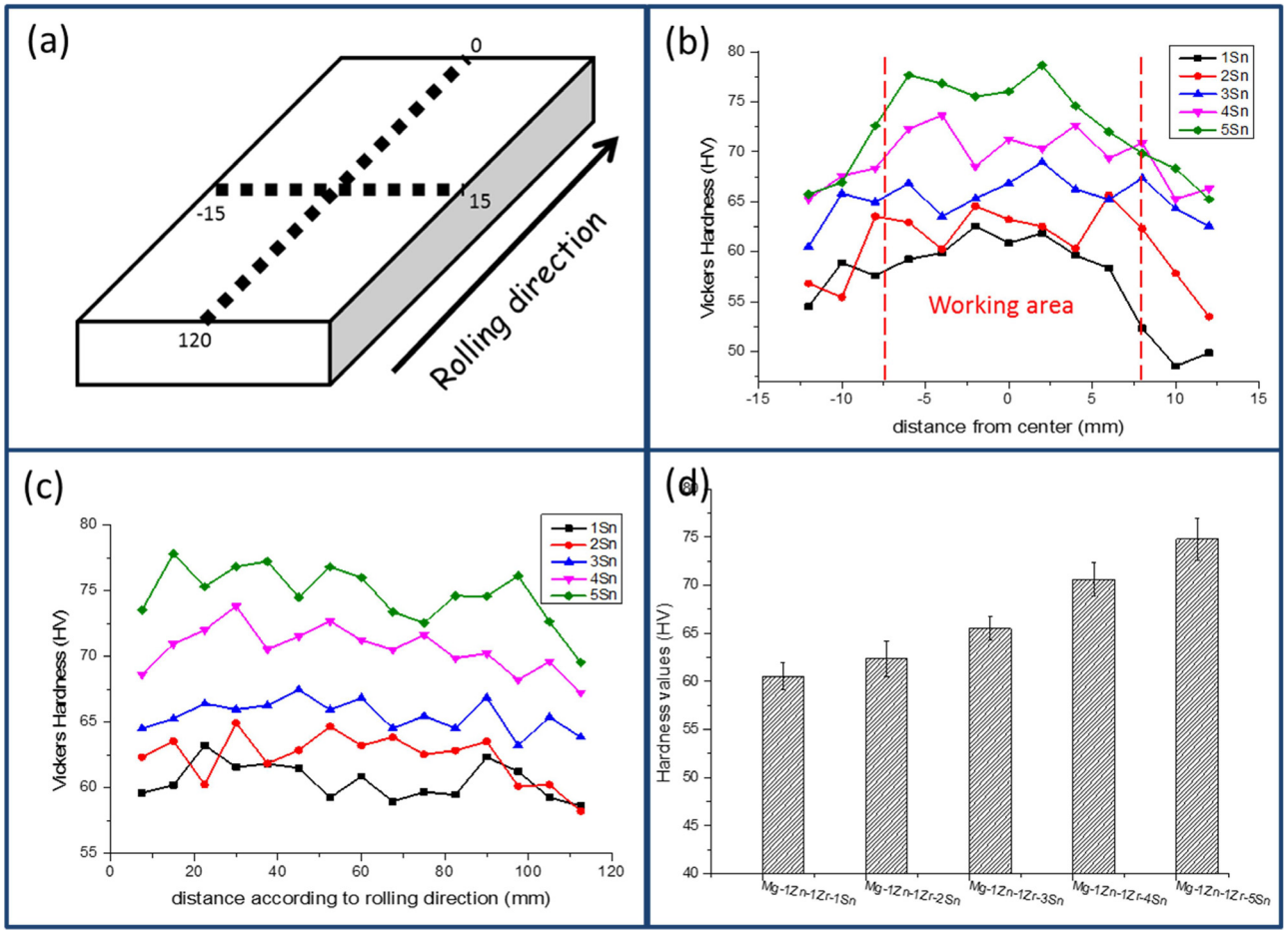

Fig. 5. (a) Schematic representation of the Vickers hardness measurement according to the rolling direction, and the Vickers hardness of the alloys according to (b) cross-sectional area, (c) along the rolling direction, and (d) average Vickers hardness of the alloys processed by PTR

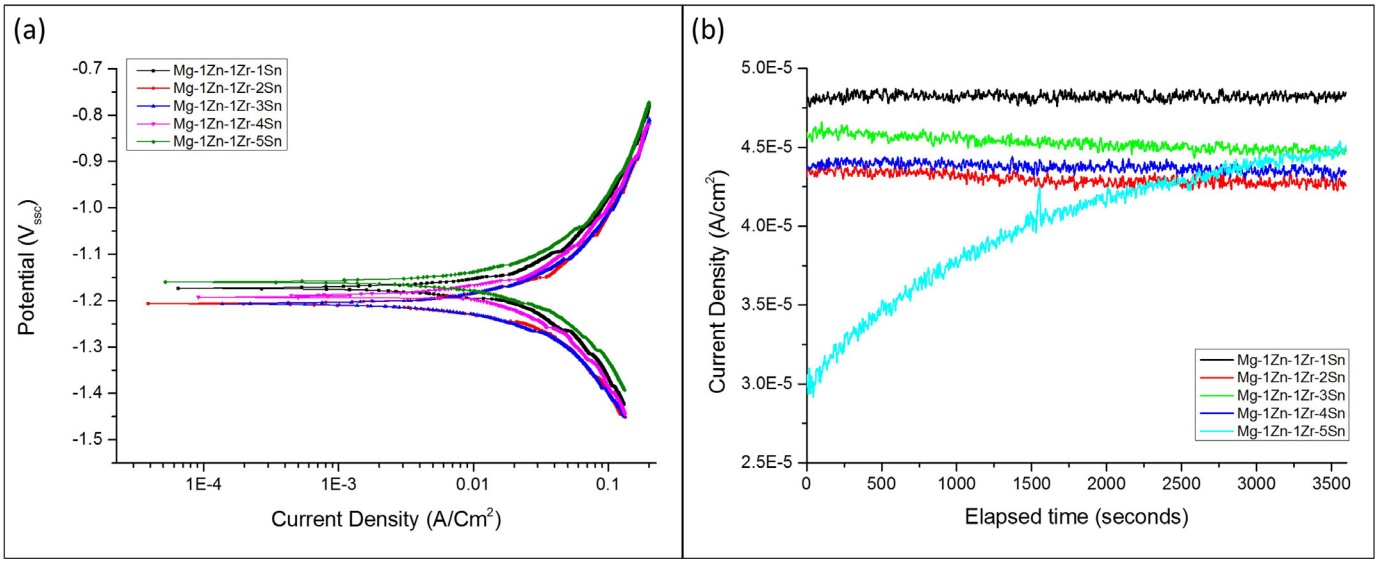

Fig. 6. (a) Potentiodynamic and (b) potentiostatic polarization test results of the PTR treated Mg-1Zn-1Zr-xSn alloys at a temperature of 37°C in Tas-SBF solution

Fig. 6 shows the potentiodynamic and potentiostatic polarization graphs of the Mg-1Zn-1Zr-xSn (x = 1, 2, 3, 4, 5 wt. %) alloys in Tas-SBF solution at a temperature of 37±1°C. The relevant parameters derived from the graph are listed in Table 4. The corrosion mechanism of the PTR treated specimen involved active dissolution, since no passivation occurred. Potentiostatic polarization tests at open circuit potential showed a fluctuation in the current density resulting from the micro-pitting of the specimens. The Mg-1Zn-1Zr-5Sn alloy had the lowest corrosion rate of 0.39 mm/year.

TABLE 4

Electrochemical parameters obtained from the potentiodynamic polarization test.

	Ecorr (Vssc)	icorr (mA/cm^2)	Corrosion rate (mm/year)
1Sn	–1.17	1.825E-02	0.42
2Sn	–1.202	1.781E-02	0.41
3Sn	–1.205	1.870E-02	0.43
4Sn	–1.195	1.91E-02	0.44
5Sn	–1.16	1.698E-02	0.39

4. Conclusions

- The PTR treated Mg alloys reached 98.3% of theoretical density and showed a fine grain size of 40.9 µm.
- The Mg_2Sn intermetallic particles were observed along the grain boundaries, while the Zn_2Zr_3 particles were distributed in the Mg matrix.
- The PTR treated Mg alloys showed increased hardness as the Sn content increased.
- The addition of 1 wt. % Sn caused the corrosion potential to shift toward a more positive value, and the resulting Mg alloy exhibited low corrosion current density.

Acknowledgements

This study was financially supported by Chonnam National University **(Grant number: 2015-2766)**.

REFERENCES

[1] M.P. Staiger, A.M. Pietak, J. Huadmai, G. Dias, Biomaterials **27**, 1728-1734 (2006).
[2] N.T. Kirkland, J. Lespagnol, N. Birbilis, M.P. Staiger, Corros. Sci. **52**, 287-291 (2010).
[3] C. Lorenz, J.G. Brunner, P. Kollmannsberger, L. Jaafar, B. Fabry, S. Virtanen, Acta Biomater. **5**, 2783-2789 (2009).
[4] C.L. Liu, Y.J. Wang, R.C. Zeng, X.M. Zhang, W.J. Huang, P.K. Chu, Corros. Sci. **52**, 3341-3347 (2010).
[5] W. Zhou, T. Shen, N.N. Aung, Corros. Sci. **52**, 1035-1041 (2010).
[6] W. He, E. Zhang, K. Yang, Mater. Sci. Eng. C **30**, 167-174 (2010).
[7] M. Yang, Y. Zhu, X. Liang, F. Pan, Z. Yi, F. Pan, Mater. Sci. Eng. A **528**, 1967-1973 (2011).
[8] J. Chen, J. Wei, H. Yan, B. Su, X. Pan, Mater. Des. **45**, 300-307 (2013).
[9] G.L. Song, Corros. Sci. **51**, 2063-2070 (2009).
[10] J. Wang, Y. Li, S. Huang, X. Zhou, Appl. Surf. Sci. **317**, 1143-1150 (2014).
[11] H. Liu, Y. Chen, Y. Tang, S. Wei, G. Niu, J. Alloys Compd. **440**, 122-126 (2007).
[12] M. Wolff, T. Ebel, M. Dahms, Adv. Eng. Mater. **12**, 829-836 (2010).
[13] B.A. Glowacki, M. Majoros, M. Vickers, J.E. Evetts, Y. Shi, I. McDougall, Supercond. Sci. Technol. **14**, 193-199 (2001).
[14] H. Kumakura, A. Matsumoto, H. Fujii, K. Togano, Appl. Phys. Lett. **79**, 2435-2437 (2001).
[15] A. Zakiyuddin, K. Lee, J. Alloys Compd. **629**, 274-283 (2015).
[16] L. Liu, X. Chen, F. Pan, Z. Wang, W. Liu, P. Cao, T. Yan, X. Xu, Mater. Sci. Eng. A **644**, 247-253 (2015).